NJC



View Article Online PAPER



Cite this: New J. Chem., 2021, 45, 2443

Received 16th November 2020 Accepted 15th January 2021

DOI: 10.1039/d0nj05603k

rsc.li/nic

Molecular design principles of ionic liquids with a sulfonyl fluoride moiety†

David J. Siegel, ‡a Grace I. Anderson, ‡a Noah Cyr, a Daniel S. Lambrecht, oa Matthias Zeller, Patrick C. Hillesheim * and Arsalan Mirjafari * * and Arsalan * and Arsalan Mirjafari * and Arsalan * a

The continued success of ionic liquids in applications ranging from energy to medicine poses the challenge to rapidly find new functional ionic liquids with desirable properties while developing practical, scalable syntheses. As a SuFExable functionality, the sulfonyl fluoride has become widely adopted throughout the field of chemical biology due, in part, to its unique stability-reactivity pattern, highlighting the underappreciated potential of the SVI-F motif in materials chemistry. For the first time, we herein report the development of a set of sulfonyl fluoride-functionalized ionic liquids with considerable structural diversity via an efficient, modular, and orthogonal fluorosulfonylethylation procedure. The resulting SO₂F-functionalized ionic milieu has properties consistent with its classification as ionic liquids. We employed a combination of molecular design, synthesis, computational modeling, and X-ray crystallographic studies to gain in-depth understanding of their structure-property correlations. The diversification of the SO₂F-bearing salts is extended to include active pharmaceutical precursors, allowing for access to functional materials with a priori low toxicity.

Introduction

As a key reagent for Sulfur(vi) Fluoride Exchange (SuFEx), 1,2 the sulfonyl fluoride group (-SO₂F) has recently reemerged as a clickable motif in medicinal chemistry,3-5 covalent probe design⁶ and drug discovery.⁷⁻⁹ The SO₂F functionality serves as a modular -SO₂- connector, joining the desired reactive moieties to the scaffold of interest, allowing for facile synthesis of larger molecular compounds. The unique reactivity of the -SO₂F functional group allows for selective and irreversible enzyme inhibition. For example, the simplest structure of this family, methanesulfonyl fluoride (MSF), was tested for the effective palliative treatment of Alzheimer's disease and was found to act as a potent inhibitor of acetylcholinesterase AChE. 10 Furthermore, PyFluor 11 is an efficient and inexpensive deoxyfluorination reagent (Fig. 1). Moreover, the relative non-reactive nature of sulfonyl fluorides was utilized to develop ¹⁸F-radiolabeled tracer compounds. ¹²

The unique reactivity of sulfonyl fluorides with nucleophiles (e.g. amino acid residues of protein binding sites) hinges upon the paradoxical combination of high kinetic barriers and robust thermodynamic driving forces. Breaking the strong SVI-F bond requires the assistance of H⁺, DBU, R₃Si⁺ or bifluoride (FHF⁻) salts^{2,13-16} under rigorous spatial and kinetic restrictions. Consequently, unlike its chloride analog, the -SO₂F unit is profoundly stable in acidic, basic, and physiological conditions. Further, sulfonyl fluorides are highly resistant toward reduction due to the SVI-F bond cleavage being exclusively heterolytic in contrast to sulfonyl chloride. The unique properties and reactivity of the -SO₂F group is perhaps best summarized by the insightful comments of K. B. Sharpless: "[SO₂F] thereby attains a hallmark of click reaction function, remaining" invisible" under most conditions and coming to life only when desired...²

Originally discovered by B. R. Baker, the desirable electrophilicity of sulfonyl fluorides enables site-specific targeting under various chemical and biological contexts, mitigating

$$H_2N$$
 H_2N
 H_2N

Fig. 1 Examples of sulfonyl fluorides as potent covalent enzyme inhibitors, and as the Doyle's deoxyfluorinating reagent.

^a Department of Chemistry and Physics, Florida Gulf Coast University, Fort Myers, Florida 33965, USA. E-mail: amirjafari@fgcu.edu

^b Department of Chemistry, Purdue University, West Lafayette, Indiana 47907, USA

^c Department of Chemistry and Physics, Ave Maria University, Ave Maria, Florida 34142, USA. E-mail: patrick.hillesheim@avemaria.edu

[†] Electronic supplementary information (ESI) available. CCDC 2032771-2032774. For ESI and crystallographic data in CIF or other electronic format see DOI: 10.1039/d0ni05603k

[‡] These authors contributed equally to this work.

off-target damage and toxicity while retaining suitable aqueous physiological stability. The hydrogen bonding (HB)-mediated reactivity-switch-on mechanism makes the reactivity of the fluoride leaving group sensitive to the microenvironment of the binding sites with the proper local HBs. As indicated by Sharpless, "...protein surfaces provide molecular information that sulfonyl fluorides are particularly adept at reading." Accordingly, the ability of sulfonyl fluorides to form covalent bonds with enzymes is highly selective compared to other electrophiles—which is the key reason for their popularity in biological contexts.

Despite the wealth of literature on sulfur(v1) oxyfluorides, their development as scaffolds for functional materials remains limited to few reports. For instance, in 2020, Xue et al. developed the "full fluorosulfonyl" electrolyte for high-voltage rechargeable lithium-metal batteries (LMBs) by dissolving lithium bis(fluorosulfonyl) imide (LiFSI) in Me₂N–SO₂F solvent. Shortly afterward, Shen et al. discovered that using Pefabloc improves performance and stability of perovskite solar cells.

Over 15 years ago, "task-specific" ionic liquids (TSILs) were first introduced by J. H. Davis as a conceptual framework for the controlled assembly of functional molecular units into an ionic liquid (IL) structure, achieving characteristic chemical behaviors.²⁰ These materials were identified as ILs where a functional group is covalently tethered to the cation and/or anion. Such ionic compounds invariably have a combination of diverse physical and chemical properties. Their inherent tunability enables the design of new functional materials, while retaining the core, desired features of conventional ILs, viz., nonvolatility, high ionic and thermal conductivity, and excellent electrochemical and thermal stability.21 A fundamental obstacle that synthetic IL chemists face is particularly clear: although ILs have moderate structural complexity, transferring synthetic organic reactions to the ionic environment remains a bottleneck due to the challenges associated with their purification (i.e. distillation, crystallization and chromatographic separation are impractical). The incorporation of new design elements (e.g. click chemistry) has led to recent advances towards novel functional IL systems.²² However, the paradigm in developing TSILs remains the incorporation of new functionalities into IL structures with great reliability as part of a linear - effective albeit slow, approach for the discovery of new functional organic materials.

It is noteworthy that until now, IL-SO₂F systems were absent from the TSILs catalog. Essentially, the combination of ILs' architectural platform and relatively sluggish reactivity of SO₂F – which we regard as an advantage rather than a liability – underpin our enthusiasm to explore the development of SO₂F-bearing ILs as a emergent class of practically useful and fundamentally interesting materials. To address the task above, we herein report the first systematic study on synthesis and empirical structure–property relationships of this new family of functional ILs.

Results and discussion

Synthesis

Three structural elements are introduced into our design: (i) the modular incorporation of various heterocyclic cations as a point for structural-core diversification *via* Menshutkin reaction to access a diverse array of ILs. (ii) In each case, we employed the non-coordinating bistriflimide anion (Tf₂N⁻) which is a widely used fluorous anion in IL formulations. Our decision is grounded in the anion's intrinsic thermal, electrochemical, and hydrolytic stability along with its aptness to form sub-ambient melting ion pairs. In fact, its high level of charge delocalization and conformational flexibility would allow us to invariably create salts with melting points as low as might be achievable. (iii) The SO₂F group acts both as a traditional functional group and a "SuFExable" site for further diversification (*i.e.* through the one-step conversion to sulphonamides, sulfonates, sulfonic acids, or sulfonyl-based dicationic ILs). This feature might be useful to covalently immobilize biomolecules (*e.g.* enzymes) on ILs for the potential development of biosensors.²³

The ease and generality of the fluorosulfonylethylation strategy was established via the preparation of a series of ethyl-linked SO₂F-functionalized ILs, illustrated in Fig. 2. We employed a variety of common imidazolium, pyridinium, 1,2,4-triazolium(aromatic), and pyrrolidinium, morpholinium (non-aromatic) cations. Further core-diversification was accomplished using electron-deficient (3c, 3d and 3i) and electron-rich (3g

Fig. 2 Two-step synthesis (top) and structures (bottom) of novel ILs $\bf 3$ constructed through the fluorosulfonylethylation of diverse heterocyclic headgroups $\bf 1$. The counter-ion of each of these cations is Tf_2N^- that is omitted for clarity. Reactions occurred at ambient temperature except $\bf 3c$, $\bf 3d$ and $\bf 3i$ required reflux condition.

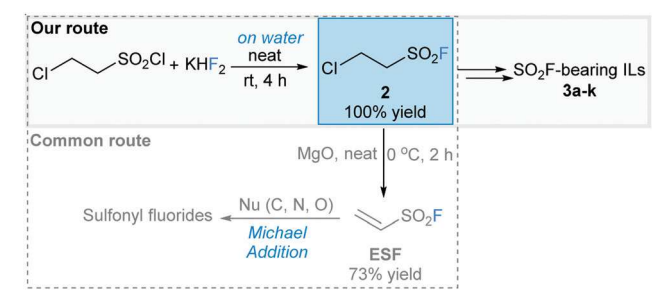
NJC

and 3h) heterocycles. Consistent with this proposal, incorporation of electron-withdrawing substitutions on the imidazolium and pyridinium rings did not lead to attenuated reactivity. Notably, the presence of various functional groups on the above-mentioned aromatic rings gives the adopted synthetic procedure an orthogonal dynamic, allowing for wide applicability of the proposed synthetic routes.

The diversification of the SO₂F-bearing salts is extended to include active pharmaceutical precursors, allowing for access to ILs with a priori low toxicity. In turn, we selected 5-nitroimidazole and 4-aminopyridine as the cations for the compounds 3c and 3g. 5-Nitroimidazole is the backbone of several antimicrobial compounds^{24,25} and 4-aminopyridine forms the core for dalfampridine (Ampyra®) which is used for the treatment of multiple sclerosis.²⁶

The IL products 3a-k were prepared via a two-step procedure based upon the N-alkylation of nitrogen-containing heterocycles 1 with 2-chloroethanesulfonyl fluoride 2, followed by anion metathesis and combining the requisite chloride salts with KNTf2 in water (Fig. 2). The formation of the IL products was confirmed by 1H, 13C and 19F NMR, MS, and by single crystal X-ray diffraction (SC-XRD). Further elaboration on synthesis and characterization of the IL products and NMR spectra can be found in the ESI.† Of particular note with respect to the NMR data is the presence of a peak at ca. -80 ppm in the 19 F spectrum of each IL, consistent with presence of an aliphatic sulfonyl fluoride group. With the exception of compounds 3c and 3d, which required elevated temperature conditions perhaps due to the presence of the deactivating nitro group, reactions were completed within few minutes at ambient temperature, indicated by the precipitation or phase separation of the products. For instance, the chloride counterparts of 3a, 3g, and 3j instantly formed precipitates upon mixing of equimolar amounts of the corresponding starting materials in ethyl acetate (see Fig. S1 in the ESI,† to see a video about the instantaneous formation of an onium chloride salt). Strikingly, purification was rarely required for each step, and the resultant IL were harvested by simple concentration and filtration or phase separation. We found that the IL products are soluble in hot water and methanol but not in methylene chloride and EtOAc (noted as useful purification solvents to separate the ILs from their precursors). Yields of both the intermediate chloride salts and the final products are quantitative. As anticipated, the ILs exhibit robust thermodynamic stability toward hydrolysis and thermolysis, making them reliable materials of choice for a diverse set of environmental conditions. All compounds were handled and stored on the benchtop for over 60 days and no elimination products (i.e. sulfenes)²⁷ were detected by ¹H and ¹³C NMR spectroscopy. Due to the facile nature of the procedure and the accessibility of starting materials, the ILs can be synthesized in multigram scale - e.g., 3a was scaled up to ca. 20 g in 94% yield.

While several synthetic routes to ethyl-linked sulfonyl fluorides were developed, a common method used in the present work is that shown in Scheme 1. Ethenesulfonyl fluoride (ESF) - "the most perfect Michael acceptor ever found",2,28 - is the most powerful SuFEx reagent to incorporate the SO₂F via the conjugate (Michael)



Scheme 1 Common (dashed box) and employed (grey box) synthetic routes to ethyl-linked sulfonyl fluorides.

addition. However, the reagent's cost (\$54.60 g⁻¹ for 95% purity) and poor shelf stability render it unsuitable for our chemistry. Strikingly, our synthetic objectives are met by using 2 (Scheme 1) in lieu of ESF. Our decision was based upon two considerations: (i) ESF is an extremely toxic substance (orally and intraperitoneally to laboratory animals§) and is a severe lachrymator that must be used under specific safety guidance; and (ii) avoid sacrificing the extraordinary efficiency of the synthesis by adding an extra step, i.e., MgO-mediated elimination with 73% yield. Described by Sharpless et al., 29 2 is readily made via the on-water sulfonyl chloride-fluoride exchange (halex process) in 100% yield, using its chloride congener and saturated KHF2 solution (Scheme 1).

Thermophysical properties

Thermophysical analysis of these ILs was carried out using thermogravimetric analysis (TGA) and differential scanning calorimetry (DSC) and the data is summarized in Table 1. Evaluating the thermal stability, the TGA data of 3a-k substantially varied between new ILs, exhibiting an initial decomposition step between 159.2–434.6 °C where $\sim 5\%$ mass loss is reached $(T_{\text{onset5\%}})$. Presumably, this indicates that the decomposition proceeds initially through the cleavage of the C-SO₂F bond (defluorosulfonylation). The thermal stability of the PyFluor-derived IL (3i) is noticeably higher than others with a $\Delta T_{\text{onset5}\%}$ between structurally related compounds 3f and 3i of 284.3 °C. We attribute this dramatic increase in stability to the interactions between to sulfonyl fluoride groups on the cation and the anion. It should be noted that thermal stability of these ILs can be modulated via incorporation of a protic functional group readily leading to formation strong HB networks. Examining the $\Delta T_{\text{onset5\%}}$ for the related series of compounds **3g** (301.8 °C), **3f** (186.3 °C), and 3h (231.6 °C) incorporation of HBs in 3g significantly increases the thermal stability as compared to the structures without the amine groups. It should be noted, however, that HBs is only one factor of many which can influence the properties of ILs.30

Evaluating the experimental values of melting points (T_m) for the ILs, all fall below the customary benchmark of 100 °C used classify a salt as an IL. Compounds 3b, 3d, 3f, 3j, and 3k are crystalline white solids with $T_{\rm m}$ values above room-temperature

 $[\]S$ The oral LD50 is approximately 50 mg kg $^{-1}$ for rats and approximately 10 mg kg $^{-1}$ for mice. The intraperitoneal LD50 is 1-5 mg kg⁻¹ for rats and <5 mg kg⁻¹ for mice. The liquid was absorbed through the intact skin, and the skin absorption LD50 is 1-5 mL kg⁻¹.²⁸

Paper NJC

Table 1 The melting point $(T_{\rm m})$, glass transition temperature $(T_{\rm g})$, and thermal decomposition temperature $(T_{\rm onset5\%})$ values of the IL products

IL	T_{m} (°C)	$T_{ m g}\left(^{\circ}{ m C} ight)$	$T_{ m onset5\%}$ (°C)
3a	_	-4.7	237.2
3b	59.6	_	184.9
3 c	_	-15.7	200.4
3d	66.4	_	159.2
3e	_	-30.2	211.9
3f	79.5	_	186.3
3g	_	_	301.8
3g 3h	_	-30.4	231.6
3i	_	18.6	434.6
3j 3k	48.9	_	229.8
3k	93.1	_	266.8

(Fig. 3). All other compounds remain as free-flowing liquids at room temperature. It is noted that the $T_{\rm m}$ peaks (onset of an exothermic peak upon heating) was only observed in the first DSC run presumably due to the high viscosity of the ILs and the tendency to form amorphous glasses instead of ordered crystalline solids even at slower cooling rate (2 °C min⁻¹). Generally, as is often the case for ILs, recrystallization on a practical timescale is not always achievable due to their dramatically increasing viscosities and the existence of supercooled states, resulting in formation of viscous glassy liquids.²¹ The remaining products exhibited no well-defined transitions from ordered solids to isotropic liquids, albeit weak, low-temperature glass transitions (T_o ; midpoint of a broad endothermic peak upon heating) were observed and these varied slightly on their thermal history (Table 1). This behavior is likely due to, in part, the symmetry of the cation frustrating solid-phase packing, resulting in the formation of a matrix that ossifies into an amorphous solid at low temperatures. 21 Predictably, we note that the presence of SO_2F has the effect of increasing the $T_{\rm m}$ values. For instance, 3b has $\Delta T_{\rm m}$ of ca. 34.6 °C, relative to the common [edmim][Tf₂N] (edmim = 1-ethyl-2,3-dimethylimidazolium), 31 which is likely due to the presence of inter- and intra-ionic interactions arising from the SO₂F group as observed in the solid-state structures. Interestingly, a comparison of the $T_{\rm m}$ values of 3b and 3d indicates that the paradoxical effects of the high polarity of NO2 and reduced π interactions (due to its electron-withdrawing nature)

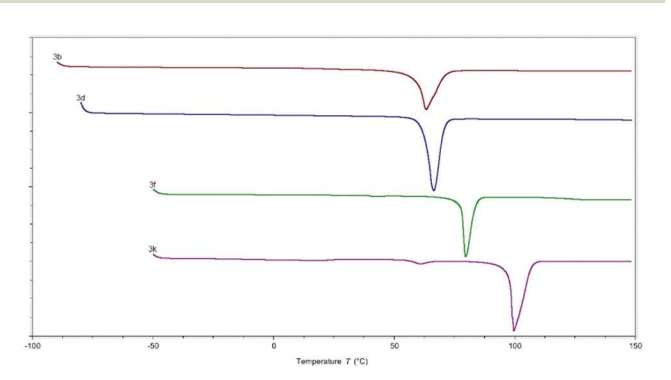


Fig. 3 DSC thermograms for compounds **3b** (red), **3d** (blue), **3f** (green), and **3k** (purple). Measurements were taken in open pans under N_2 gas at ramp rate of 5 °C min⁻¹. The thermograms have been offset for clarity, but not rescaled.

result in a slight increase in $T_{\rm m}$ of 3d ($\Delta T_{\rm m}$ = 3.0 $^{\circ}$ C) in comparison to 3h.

To further provide insight toward into structure–property relationships of the new ILs, the dynamic and kinetic viscosity, and density of a representative IL (3a) was measured as function of temperature at 1 bar and are shown in Fig. 4 and Table S1 (see ESI†). As anticipated, the incorporation of sulfonyl fluoride functionality has great influence on the viscosity of 3a relative to a corresponding IL with all-carbon and the same number of side-chain backbone atoms, *i.e.*, [emim][NTf₂] has a η value of 34.0 mPa s³² compared to 3a with η value of 1081.9 mPa s s at 20 °C. It is consistent with increased inter-particle interaction brought upon by the grafting of the powerfully associating functional groups. For many ILs, viscosity is a strong function of temperature near room temperature, as is the case for representative IL, with viscosity varying over *ca.* 27 orders of magnitude in the temperature range studied.

X-ray crystallography

To better understand the structural impact incorporation of the SO₂F group has on the compounds, we conducted crystallographic analysis allowing for direct insight into the spatial relationship between the cations and the anion as well as enhanced understanding of their physicochemical properties. Typically, due to the conformational freedom of the Tf₂N⁻ anion, ILs with this anion display complex crystallization behavior and growing diffraction quality crystals is very challenging.³³ However, we succeeded in forming suitable crystals of 3b, 3c and 3f for SC-XRD study and their asymmetric units are depicted in Fig. 2 and 5. The presence of the SO₂F group results in intermolecular interactions that encourages crystallization perhaps due to its high polarity. Despite considerable efforts, unfortunately, we were unable to produce the crystals of other IL products of suitable quality. In turn, we isolated a crystal from the cognate of 3a, paired with BETI (bis[(pentafluoroethyl)sulfonyl]imide) anion, confirming the formation of the corresponding SO₂Fbearing imidazolium cation (Fig. 5). It should be noted that we prepared the BETI⁻ analog of 3a because we had ready access to a stock of LiBETI, a relatively hard-to-acquire material.

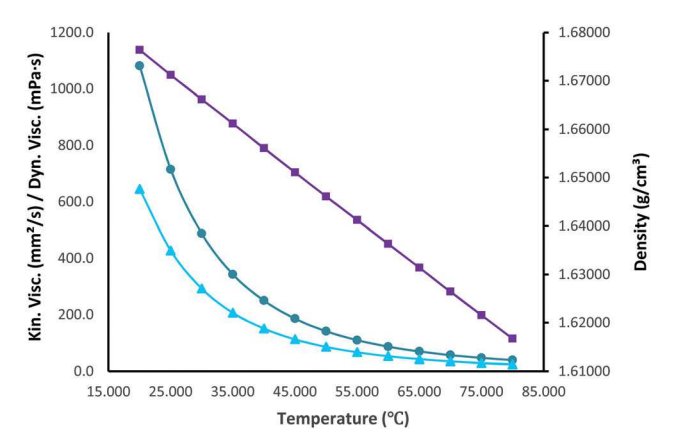
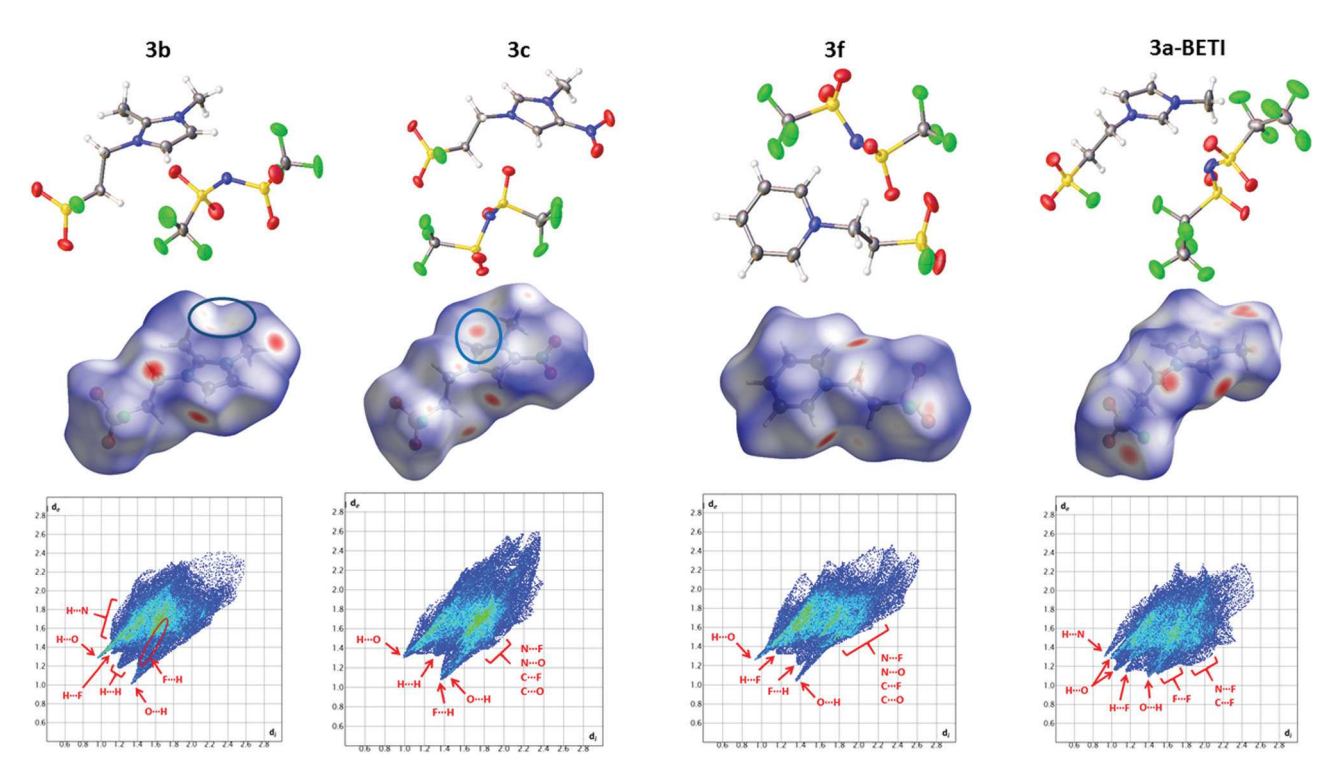


Fig. 4 The dynamic (blue) and kinetic (teal) viscosity, and density (purple) of IL **3a**.

NJC



Top row: the asymmetric units of 3b, 3c, 3f and 3a - BETI salts. Middle row: dnorm mapped on the Hirshfeld surfaces. Bottom row: Fingerprint

Further, to seek greater insight into intermolecular interactions within a crystal structures, we concluded that a solid-state Hirshfeld surface analysis of these new materials would be useful. Several important insights emerge from the obtained data as depicted in Fig. 5. Hirshfeld surface analysis is performed via the CrystalExplorer. Hirshfeld surface analysis is a "whole molecule approach" to examining the intermolecular interactions and packing mode within a crystal structure.34,35 In brief, the Hirshfeld surface mapped with d_{norm} allows for facile visualization of interactions outside (d_e) and within (d_i) the boundaries of the surface. The exact definitions of d_i , d_e , and d_{norm} are provided within the relevant literature and are defined, briefly, herein. 34,36,37 The color coding on the Hirshfeld surface, that is blue to white to red, indicate relative distances of interactions, with blue indicating distances longer the sum of the van der Waals radii and red being less than the sum of the radii. These interactions can be deconstructed into two dimensional plots of d_i and d_e known as fingerprints.³⁷ These fingerprint plots not only allow for qualitative comparisons based on shape and structural features of the plot, but can also be broken down to a 'per atom' basis allowing for granular, percentage-based comparisons of interactions arising from distinct sets of atoms within a structure. The fingerprint plots and Hirshfeld surfaces, along with a traditional approach to crystallographic analysis, allows for a wealth of information to be extracted from the structure of compounds. Particularly, they provide direct insight into the spatial relationships between the cation and anion and structural features of the ILs, providing a strong basis to further understand both short range (e.g. H-bonding) and coulombic interactions.³⁸ The surfaces and fingerprint plots for the crystal structures are shown in Fig. 5 and Table S2 (see ESI†) contains the relative percentages of interactions obtained from the fingerprint plots. In an effort to evaluate the impact the SO₂F groups have on the solid-state structure, discussion presented herein focuses predominantly on analysis of the cationic portions of the structures only.

Crystallographic data for IL 3b. 3b crystals crystallize in the $P\bar{1}$ space group with a single ion pair in the asymmetric unit (see ESI,† Table S3). Both the cation and anion are disordered (solvable) over two positions with the larger component of the disorder accounting for approximately 90% occupancy. The major portion of the disorder was isolated and used for surface analysis. Examining the fingerprint plot of the cation, one can see the expected peaks arising from H···O|O···H reciprocal H-bonding at $d_{\rm i} \approx 0.9, d_{\rm e} \approx 1.3$, as well as at the reciprocal distances.³⁷ The shortest of these interactions are between the hydrogens on the ring, namely C4-H, and the sulfonyl oxygens on the anion (d = 2.3469(17) Å) followed by the O···H-C interactions (d = 2.38-3.56 Å) with symmetry adjacent anions.

A number of cation-cation interactions arising from both the oxygens and fluorine atoms in the SO₂F group can be seen as the red spots on the Hirshfeld surface. As seen with compounds 3a-BETI and 3c (vide infra) the sulfonyl oxygen atoms are linking cations together through H···O···H chains with interactions ranging from 2.4783(12) Å to 3.1029(11) Å. However, the cation-cation interactions in 3b are distinct. While there are the H···O···H chains linking the cations, the sulfonyl oxygens are also bridging with the π cloud of the adjacent cations, interacting specifically with the nitrogen in the cation.^{39,40}

This interaction is seen as a 'pocket' in the surface and is highlighted in Fig. 5.

The fluorine atom of the SO₂F also contributes to several cation-cation interactions, the shortest of which are between the fluorine and several hydrogens on both the ring and ethylene chain. The closest interactions are with the C4-H on the imidazolium ring at distances of 2.7688(10) Å, forming a sort of dimeric, paired cation motif. These interactions are unique from those observed in the other compounds as the fluorine appears to only form the dimers rather than link cations together in a chain-type structure.

Crystallographic data for IL 3c. 3c crystallizes in the $P2_1/c$ space group with a single cation-anion pair in the asymmetric unit with no disorder observed in either moiety (see ESI,† Table S4). With the inclusion of the nitro group on the imidazole cation one can see two bright red spots near one of the nitrogen atoms in the heterocycle indicating an interaction with the π system of the ring (circled in Fig. 5). These interactions are seen in the fingerprint plot as the wing-type structure near $d_i \approx 1.9$, $d_{\rm e} \approx 1.5.^{41,42}$ While all the other cations do exhibit these π -type interactions, to a varying degree, 3c is the only one to display a defined feature in the plot. Further, examining Table S2 (ESI†) shows that 3c has the lowest percentage of H...H interactions of the three imidazolium compounds examined, despite having only one less hydrogen when compared to 3a-BETI (vide infra). The decreased percentage of H···H interactions is easily seen when contrasting the fingerprint plots of 3b versus 3c (Fig. 5).

The sulfonyl fluoride interactions in IL 3c are also unique when compared to the other imidazolium-based structures. Specifically, while the fluorine atom is acting as a bridge between cations as observed in 3a, the points of interaction are unique with $F \cdot \cdot \cdot H - C6$ (d = 2.589(2) Å) and $F \cdot \cdot \cdot H - C7$ (d = 2.589(2) Å) 3.153(2) Å). Additionally, the oxygen atoms are seen bridging cations through interactions with the C6-H methyl group and the C7-H methylene groups in similar manners discussed with compounds 3a and 3b. The distances of these interactions are also comparable, ranging from about 2.53-2.68 Å.

As expected, however, the percentage of interactions originating from oxygen is the highest of all the compounds examined. This is also noticeable when looking at the difference in shape of the H-bonding spikes from the fingerprints. While ILs 3b and 3c share some similarities, 3c is unique in several ways. For example, the $H \cdot \cdot \cdot O | O \cdot \cdot \cdot H$ peaks in 3c are much wider than in the other structures, accounting for the increased percent contribution of oxygen to the overall interactions. Further, looking at the fingerprints as a whole, the interactions in 3c are more dense, especially at the longer d_i/d_e values. Disperse interactions are theorized to indicate suboptimal crystal packing⁴² but are a common feature in fingerprints of ILs with the Tf₂N anion.⁴¹

Crystallographic data for IL 3f. 3f crystallizes in the $P\bar{1}$ space group with a four cation-anion pairs in the asymmetric unit (Z' = 4, Z = 8) (see ESI,† Table S5). While structures of ILs have been previously reported with similar Z' values, ^{43,44} the structure reported herein is the first example of a pyridinium IL with Z' = 4containing the Tf₂N⁻ anion. Following on this, all four of the individual cations in the asymmetric unit display unique fingerprints (see ESI,† Fig. S2). The discussion herein will pertain only to cation C, however it can be extended to some degree to all of the cations.

The pyridinium-based IL offers a chance to examine interactions of the sulfonyl fluoride group with a non-imidazolium based set of aromatic hydrogens. The Tf₂N⁻ anion shows strong interactions with the α hydrogens, that is C1-H and C5-H, of the pyridinium ring. Further, the anion also has the shortest interactions with the methylene hydrogens on the alkyl chain at distances of 2.35 Å to 3.01 Å. These interactions are seen as the bright red spots near the relevant hydrogens on the Hirshfeld surface in Fig. 5. The sulfonyl fluoride oxygens on the cation show longer-distance interactions with the β hydrogens (C2-H & C4–H) and γ hydrogens (C3–H) at distances of approximately 3.0 Å. These interactions exist between several of the crystallographically unique cations within the asymmetric unit. The shortest O···H interaction, however, is at 2.500(2) Å between cation C and cation B and is seen as the H-bonding spike at d_i \approx 1.4, $d_{\rm e} \approx$ 1.1. As is observed with the imidazolium-based cations, the SO₂F moiety bridges aromatic hydrogens in the typical H···O···H chain manner.

As seen by the red spot near the fluorine atom in the SO₂F group, the fluorine atom has several close contacts with hydrogens on adjacent cations. Specifically, the fluorine is interacting with the γ hydrogen on cation A at a distance of 2.635(2) Å. These interactions are also seen by a set of $H \cdot \cdot \cdot F | F \cdot \cdot \cdot H$ peaks noted in the fingerprint plot.

Crystallographic data for BETI analog of 3a. The 3a-BETI compound ($T_{\rm m}$ = 39.6 °C; $T_{\rm g}$ = -12.8 °C; $T_{\rm onset5\%}$ = 274.0 °C) crystallizes in the $P2_1/c$ space group with a single cation-anion pair in the asymmetric unit (see ESI,† Table S6). The BETI anion is disordered over multiple points by rotation. The Hirshfeld surface for the cation was calculated with all portions of the disordered anion as part of the structure, likely giving rise to some of the disperse sets of interaction points seen along the boundaries of the fingerprint plot. The fingerprint plot for the cation shows a number of defining features, which are shared among all of the cations examined, including a number of H-bonding spikes and a wing-type structure characteristic of interactions with the π cloud of the heretocycle.³⁷

Interactions with the methylene and methyl hydrogens on the ancillary chains comprise the majority of the H...O interactions seen in the spikes at $d_{\rm i} \approx 1.0$, $d_{\rm e} \approx 1.2$ –1.3. These interactions are clearly seen as the red spots on the surfaces surrounding the appropriate regions on the cation. As indicated in Fig. 5, there are two distinct H...O peaks, one larger diffuse peak in blue and one sharper peak in green. The larger blue peak arises from interactions between the methylene hydrogens and the disordered sulfonyl oxygens of the anion. Additional interactions are from close-contacts with a non-disordered portion of the anion. Overall, the H...O interactions from the methylene hydrogens to the sulfonyl oxygens on the BETI anion range from approximately 2.36 Å to 2.70 Å, bearing in mind the disordered parts of the anion.

Focusing specifically on interactions arising from the SO₂F moiety on the cation, there are O···H and F···H interactions

observed at $d_i \approx 1.4$, $d_e \approx 1.2$. As detailed in Table S2 (ESI†), interactions arising from the sulfonyl oxygens constitute 19.7% of the total interactions while the fluorine atom contributes to 9.0%. Both oxygens, that is O1 and O2, are interacting with distinct, symmetry adjacent cations. The closest interactions are between the oxygen atoms and the hydrogens on C4-H, C5-H, and C6-H at distances ranging from 2.56 Å to 2.72 Å. The sulfonyl oxygens act as bridges, linking multiple cationic units together through H···O···H chains. The fluorine is also interacting with the hydrogens on the methyl group (C6-H), acting as a bridge between cations via the methyl group C6-H at distances ranging from 2.5991(14) Å up to 3.0630(15) Å. These F...H interactions are another common trait observed in the cations and are manifested by the blunted H-bonding spikes indicated in Fig. 5.

Overall, examining all of the structures presented herein, O···H and F···H interactions from the sulfonyl fluoride moiety add a significant quantity of cation-cation interactions that is not present in simple alkyl-based ILs. The percentages listed in Table S2 (ESI†) show that inclusion of SO₂F moieties added approximately 20% intermolecular interactions arising from the oxygen and about 8% of interactions from the fluorine. Given that the shortest, and thus the strongest of these interactions are due to hydrogen atoms, the increased crystalline nature of the SO₂F-bearing ILs can likely be attributed to increased hydrogen interactions between cations. It should be noted, however, that not all the interactions may be favorable as both the fluorine and oxygen atoms exhibit potentially unfavorable $O \cdot \cdot \cdot O$, $O \cdot \cdot \cdot F$, $F \cdot \cdot \cdot F$ interactions in all crystals examined.⁴⁵

Several bridging motifs are observed in the four structures arising from both the oxygen and fluorine atoms in the SO₂F moiety. Interactions were observed between aromatic and aliphatic hydrogen atoms. Further, these interactions appear to be competitive with the anion. Specifically, the donor atoms on the cation -SO₂F group and the anion are very similar. Granted, the anionic S=O groups will have a higher negative charge thus making them more likely HB acceptors. Further, several $O/F \cdots \pi$ interactions arising from the cations were also seen arising from the SO₂F moiety, which are again similar to those observed arising from the SO₂ groups on the Tf₂N⁻ anions.

Computational approach

In tandem with X-ray analysis, since several computational approaches were performed to study (and predict) the ILs' properties as both function of the cation structure and the anion identity, it seemed reasonable to do so with one of the synthesized ILs. Accordingly, density functional theory predictions were performed to confirm and interpret experimental findings and to predict properties of 3b. To this end, the ωB97X-D dispersion-correct range-separated functional was employed in combination with the polarization consistent (pc) family of basis sets of double- and triple-zeta quality (pc-1 and pc-2, respectively). 46,47 ωB97X-D yields accurate energetics and geometries across a broad range of benchmarks, including for example non-covalent interactions which are reproduced typically within a root mean square deviation of 1-2 kcal mol⁻¹.⁴⁸ The

polarization consistent basis set family was designed to enable systematic improvement of energetics for self-consistent field approaches,⁴⁷ similar in spirit to the correlation-consistent basis set family for correlation energies. 49

Initial geometries for structure prediction were obtained from the crystal structures reported in this work. Our predictions included one cation-anion pair excised from the crystal structure of 3b either treated in vacuum for exploratory calculations and comparison or using the "conductor-like" polarizable continuum model (C-PCM) to incorporate solvent effects. 50,51 Since this work is the first to present results on 3b, a range of dielectric constants for use in the C-PCM treatment was tested to assess the impact on predicted properties. Based on published results for loosely related ILs,52 three dielectric constants were included to bracket the estimated constant for the system ($\varepsilon_r = 6$, 12, 24). Starting with the initial geometries and solvent treatment as just described, molecular geometries were optimized at the ωB97X-D/pc-1 level of theory. Subsequent property calculations, such as dipole moments, polarizabilities, and electrostatic potential maps were calculated at the ωB97X-D/pc-2 level. All ωB97X-D/pc-1 and ωB97X-D/pc-2 calculations were performed with a development version of the Q-Chem program package.⁵³ Dielectric constants were predicted at the BP86/def2-TZVP level of theory^{54,55} following a computational approach proposed by the Krossing group.⁵⁶ These calculations were performed both within Q-Chem and with the Orca quantum chemistry program packages.57,58

The computationally predicted geometries are in good agreement with the experimentally obtained crystal structures (Table 2). For example, using the shortest cation-anion distance as a representative geometric measure, the distance between the N-Me on the imidazolium ring and the nitrogen of the NTf₂ anion, computational predictions produce between 3.013 and 3.079 Å compared to 3.345 Å in the experiment. Likewise, other geometric parameters agree well with the experimental findings (see ESI,† Tables S7-S12). This agreement between experiment and theory is encouraging, as it suggests sufficiently accurate modelling at least of short-range interactions and confirms experimental assignments.

The predicted dipole moments range between 16.7 and 18.2 Debye (excluding the vacuum result) and depend on the C-PCM dielectric constant used. As expected, embedding the ion pair in a more polar dielectric environment leads to an increase in predicted dipole moment due to stabilization of polarization.

Table 2 Computationally predicted properties for 3b depending on the solvent dielectric constant employed in the C-PCM treatment. R denotes the shortest cation/anion distance, q(e) denotes the charge on the cation taken as the sum of the Mulliken charges. Deviations from the integer (+1) charge provide an estimate of the extent of charge transfer between the cation-anion pair

Solvent ε_{r}	R (Å)	Total dipole (Debye)	Polarizability (Bohr ³)	q (e)
1 (vacuum)	3.013	13.7	198.9	0.9621
6	3.013	16.7	198.3	0.8935
12	3.013	17.1	198.3	0.8936
24	3.079	18.2	198.6	0.9042

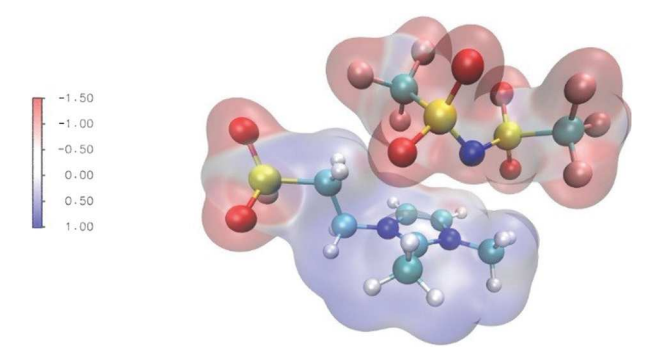


Fig. 6 Electrostatic potential map. Electrostatic potentials were calculated at the B3LYP/pc-2 level of theory 54,59,60 on a 300 \times 240 \times 200 grid with approx. 20 grid points per Angstrom. Plots were created in the VMD graphical interface. 61 Shown is the ESP on an electron density isosurface with contour value 0.1

On the other hand, the predicted polarizabilities do not show a significant dependence on the polarity of the environment. The overall sizable dipole moment becomes apparent from the electrostatic potential (ESP) plot showing a pronounced positive potential over the imidazolium ring of the cation and pronounced negative potential regions distributed over the anion (Fig. 6). A noteworthy exemption is that the SO₂F moiety on the cation also shows negative electrostatic potential, as expected based on the electronegativity of the atoms involved. A region of pronounced negative ESP on the cation of an IL is unusual and can be expected to lead to short-ranged intermolecular interactions not typically found with the cations of an IL.

The predicted charges for the cation range between 0.8935 and 0.9042 electron charges depending on the dielectric constant used for the C-PCM (again omitting the vacuum results as a special case). This result corresponds to a transfer of electron density between the cation and anion ranging between 0.0958 and 0.1065 electrons depending on the polarity of the solvent environment. While Mulliken charges are basis set dependent and should not be interpreted as absolute numbers, the magnitude of deviation from the integer (+1) charge suggests that there is a considerable transfer of electron density between the cation and anion and indicates an electronic interaction between the cation and anion that goes beyond pure electrostatics.

We have predicted dielectric constants of 3b based on the computational approach presented by the Krossing et al.,56 which is based on a fit of computationally predicted descriptors to experimental dielectric constants for a range of ILs. Specifically, the dielectric constant was calculated from the equation:

$$\varepsilon_{\rm r} = a + b \frac{V_{\rm m}}{V_0} + c \frac{\Delta G_{\rm s}}{G_0}$$

where a = -97.8, b = 51.4, c = 0.206 were determined by Krossing and co-workers. 56 $V_{\rm m}$ is the molecular volume obtained from density functional theory prediction and $V_0 = 1 \text{ nm}^3$. ΔG_s is the solvation energy again obtained from the solvent model and $G_0 = 1 \text{ kJ mol}^{-1}$. Note that the sign of constant c is flipped compared to the definition of Krossing et al., which was necessary to reproduce the previously published results.56

We also note that due to differences in our software we modified the approach compared to the one presented by the Krossing group.⁵⁶ Specifically, we used the C-PCM solvation model and not COSMO⁶² as in the originally proposed method and used in-house Python code to determine molecular volumes utilizing the Mendeleev package¶ to import atomic radii. Moreover, solvation energies were obtained for cation-anion pairs combined. Due to the differences between our computational approaches, some of the calculated parameters differed from those of Krossing and co-workers.⁵⁶ However, we found that scaling of the parameters led to good agreement with the published results. Specifically, we scaled our molecular volumes and solvation energies, respectively (see ESI,† Tables S13-S15). With these adjustments, our computational approach provided an excellent reproduction of the published results⁵⁶ for a combined training/test set of seven ILs with a root mean square deviation of 1.3 units in the dielectric constant (Table S16, ESI†).

Using this approach, we obtained a dielectric constant of 26.8 for 3b, which places 3b in the upper range for dielectric constants among reported values because of the presence of the sulfonyl fluoride group. We note that it is not yet clear whether these predictions based on an empirical analysis between computational descriptors and experimental dielectric constants are transferable to 3b structure and electrostatic properties. However, at the very least we believe the result further emphasizes the unique properties of 3b.

Conclusions

Fundamental to the field of ILs is the understanding that structure begets function. For the first time, we developed a series of novel task-specific ILs containing a sulfonyl fluoride moiety, as a thermally stable and chemical robust functionality. Generally, the SO₂F functionality is much more thermodynamically stable than other sulfonyl halides toward hydrolysis, reduction, and thermolysis.² Along with its biocompatibility, these features incentivize the investigation and development of sulfonyl fluorides and allude to the reasoning behind their successful inclusion in drug development applications. In this work, eleven structurally diverse IL-SO₂F systems, including three containing biologically active cores were synthesized in gram-quantity scale. Using active pharmaceutical ingredients (APIs) with established toxicological profiles and the biocompatible SO₂F group may serve to develop ILs with reduced toxicity. The products can be simply scaled-up without sacrificing their yields or purity. To aid defining their practical range of use for various applications, the thermophysical properties of new ILs, including melting points, glass transition temperatures, thermal stability, density, and temperaturedependent viscosity were reported.

Aside from providing a practical route to ILs with useful properties, the exceptionally facile synthetic procedure allowed us to produce the ILs with great reliability through a consistent, well-controlled pathway. Simple reaction conditions and non-

[¶] L. M. Mentel, mendeleev - A Python resource for properties of chemical elements, ions and isotopes, available at: https://github.com/lmmentel/mendeleev.

chromatographic purification procedures were employed with quantitative yields throughout. Despite the common practice of using ESF as a highly reactive Michael acceptor to prepare ethyllinked sulfonyl fluorides, we chose an alternative method, allowing efficient and rapid access to diverse SO₂F-bearing ILs and bypassing the higher costs and toxicity associated with ESF as a raw material. The synthetic technique presented herein is a facile approach for creating a wide variety of SO₂Ffunctionazlied low-melting salts and is integral to the progression of the rapidly expanding field. And, since we have recently begun to elucidate the types of modifications that can be made to SO₂F-IL systems without compromising their melting point, we expect in our future work to exploit this knowledge to prepare variants of the sulfur(vi) oxyfluoride ILs.

Conflicts of interest

NJC

There are no conflicts to declare.

Acknowledgements

This material is based upon work supported by the National Science Foundation under Grant No. CHE-1952846 (RUI), and CHE-1919785 and CHE-1625543 (MRI). Acknowledgment is made to the Donors of the American Chemical Society Petroleum Research Fund for partial support of this research. A. M., D. J. S. and G. I. A. are grateful for the generous supports provided by the Brodie and Blair Foundation Scholarships, administered by the Whitaker Center. A. M. thanks Professor Jim Davis at University of South Alabama for generously providing a stock of LiBETI.

Notes and references

- 1 W. Steinkopf, J. Prakt. Chem., 1927, 117, 1-82.
- 2 J. Dong, L. Krasnova, M. G. Finn and K. B. Sharpless, Angew. Chem., Int. Ed., 2014, 53, 9430-9448.
- 3 A. Narayanan and L. H. Jones, Chem. Sci., 2015, 6, 2650-2659.
- 4 O. Fadeyi, M. D. Parikh, M. Z. Chen, R. E. Kyne Jr., A. P. Taylor, I. O'Doherty, S. E. Kaiser, S. Barbas, S. Niessen, M. Shi, S. L. Weinrich, J. C. Kath, L. H. Jones and R. P. Robinson, ChemBioChem, 2016, 17, 1925-1930.
- 5 E. C. Hett, H. Xu, K. F. Geoghegan, A. Gopalsamy, R. E. Kyne, C. A. Menard, A. Narayanan, M. D. Parikh, S. Liu, L. Roberts, R. P. Robinson, M. A. Tones and L. H. Jones, ACS Chem. Biol., 2015, 10, 1094-1098.
- 6 L. H. Jones and J. W. Kelly, RSC Med. Chem., 2020, 11, 10-17.
- 7 B. R. Baker, Acc. Chem. Res., 1969, 2, 129-136.
- 8 Z. Liu, J. Li, S. Li, G. Li, K. B. Sharpless and P. Wu, J. Am. Chem. Soc., 2018, 140, 2919-2925.
- 9 C. Sadlowski, B. Park, C. Araujo Borges, S. Das, D. Lucas Kerr, M. He, H. Han, L. Riley and N. Murthy, Mol. Syst. Des. Eng., 2018, 3, 599-603.

- 10 D. E. Moss, R. G. Fariello, J. Sahlmann, I. Sumaya, F. Pericle and E. Braglia, Br. J. Clin. Pharmacol., 2013, 75, 1231-1239.
- 11 M. K. Nielsen, C. R. Ugaz, W. Li and A. G. Doyle, J. Am. Chem. Soc., 2015, 137, 9571-9574.
- 12 J. A. H. Inkster, K. Liu, S. Ait-Mohand, P. Schaffer, B. Guérin, T. J. Ruth and T. Storr, Chem. - Eur. J., 2012, 18, 11079-11087.
- 13 B. Gao, L. Zhang, Q. Zheng, F. Zhou, L. M. Klivansky, J. Lu, Y. Liu, J. Dong, P. Wu and K. B. Sharpless, Nat. Chem., 2017, 9, 1083-1088.
- 14 T. Hmissa, X. Zhang, N. R. Dhumal, G. J. McManus, X. Zhou, H. B. Nulwala and A. Mirjafari, Angew. Chem., Int. Ed., 2018, 57, 16005-16009.
- 15 T. Guo, G. Meng, X. Zhan, Q. Yang, T. Ma, L. Xu, K. B. Sharpless and J. Dong, Angew. Chem., Int. Ed., 2018, 57, 2605-2610.
- 16 J. Dong, K. B. Sharpless, L. Kwisnek, J. S. Oakdale and V. V. Fokin, Angew. Chem., Int. Ed., 2014, 53, 9466-9470.
- 17 T. Fujigaya, Y. Sibasaki, S. Ando, S. Kishimura, M. Endo, M. Sasago and M. Ueda, Chem. Mater., 2003, 15, 1512-1517.
- 18 W. Xue, Z. Shi, M. Huang, S. Feng, C. Wang, F. Wang, J. Lopez, B. Qiao, G. Xu, W. Zhang, Y. Dong, R. Gao, Y. Shao-Horn, J. A. Johnson and J. Li, Energy Environ. Sci., 2020, 13, 212-220.
- 19 C. Shen, Y. Wu, S. Zhang, T. Wu, H. Tian, W.-H. Zhu and L. Han, Solar RRL, 2020, 4, 2000069.
- 20 J. J. H. Davis, Chem. Lett., 2004, 33, 1072-1077.
- 21 D. R. MacFarlane, M. Kar and J. M. Pringle, Fundamentals of Ionic Liquids: From Chemistry to Applications, Wiley-VCH Verlag GmbH & Co. KgaA, 2017.
- 22 A. Mirjafari, Chem. Commun., 2018, 54, 2944-2961.
- 23 F. Ghorbanizamani and S. Timur, Anal. Chem., 2018, 90, 640-648.
- 24 D. I. Edwards, J. Antimicrob. Chemother., 1993, 31, 9-20.
- 25 Y. Miyamoto, J. Kalisiak, K. Korthals, T. Lauwaet, D. Y. Cheung, R. Lozano, E. R. Cobo, P. Upcroft, J. A. Upcroft, D. E. Berg, F. D. Gillin, V. V. Fokin, K. B. Sharpless and L. Eckmann, Proc. Natl. Acad. Sci. U. S. A., 2013, 110, 17564-17569.
- 26 S. Sedehizadeh, M. Keogh and P. Maddison, Clin. Neuropharmacol., 2012, 35, 191-200.
- 27 J. F. King, Acc. Chem. Res., 1975, 8, 10-17.
- 28 Q. Chen, P. Mayer and H. Mayr, Angew. Chem., Int. Ed., 2016, 55, 12664-12667.
- 29 Q. Zheng, J. Dong and K. B. Sharpless, J. Org. Chem., 2016, 81, 11360-11362.
- 30 C. Roth, T. Peppel, K. Fumino, M. Köckerling and R. Ludwig, Angew. Chem., Int. Ed., 2010, 49, 10221-10224.
- 31 R. Tao, G. Tamas, L. Xue, S. L. Simon and E. L. Quitevis, J. Chem. Eng. Data, 2014, 59, 2717-2724.
- 32 M.-J. Deng, P.-Y. Chen, T.-I. Leong, I. W. Sun, J.-K. Chang and W.-T. Tsai, Electrochem. Commun., 2008, 10, 213-216.
- 33 R. A. O'Brien, M. S. Zayas, S. T. Nestor, J. C. Gaitor, L. M. Paul, F. A. Edhegard, S. Minkowicz, R. E. Sykora, Y. Sheng, S. F. Michael, S. Isern and A. Mirjafari, New J. Chem., 2016, 40, 7795-7803.
- 34 M. A. Spackman and D. Jayatilaka, CrystEngComm, 2009, 11, 19-32.

- 35 J. J. McKinnon, A. S. Mitchell and M. A. Spackman, Chem. -Eur. J., 1998, 4, 2136-2141.
- 36 J. J. McKinnon, D. Jayatilaka and M. A. Spackman, Chem. Commun., 2007, 3814-3816.
- 37 J. J. McKinnon, M. A. Spackman and A. S. Mitchell, Acta Crystallogr., Sect. B: Struct. Sci., 2004, 60, 627-668.
- 38 P. M. Dean, J. M. Pringle and D. R. MacFarlane, Phys. Chem. Chem. Phys., 2010, 12, 9144-9153.
- 39 S. K. Singh and A. Das, Phys. Chem. Chem. Phys., 2015, 17, 9596-9612.
- 40 S. M. Malathy Sony and M. N. Ponnuswamy, Cryst. Growth Des., 2006, 6, 736-742.
- 41 P. M. Dean, J. M. Pringle, C. M. Forsyth, J. L. Scott and D. R. MacFarlane, New J. Chem., 2008, 32, 2121-2126.
- 42 M. A. Spackman and J. J. McKinnon, CrystEngComm, 2002, 4, 378-392.
- 43 D. Rauber, F. Heib, M. Schmitt and R. Hempelmann, J. Mol. Liq., 2016, 216, 246-258.
- 44 X. Han, J. Ke, N. Suleiman, W. Levason, D. Pugh, W. Zhang, G. Reid, P. Licence and M. W. George, Phys. Chem. Chem. Phys., 2016, 18, 14359-14369.
- 45 K. Reichenbächer, H. I. Süss and J. Hulliger, Chem. Soc. Rev., 2005, 34, 22-30.
- 46 J.-D. Chai and M. Head-Gordon, Phys. Chem. Chem. Phys., 2008, 10, 6615-6620.
- 47 F. Jensen, J. Chem. Phys., 2001, 115, 9113-9125.
- 48 N. Mardirossian and M. Head-Gordon, Mol. Phys., 2017, **115**, 2315-2372.
- 49 T. H. Dunning Jr., J. Chem. Phys., 1989, 90, 1007-1023.
- 50 T. N. Truong and E. V. Stefanovich, Chem. Phys. Lett., 1995, **240**, 253-260.
- 51 M. Cossi, N. Rega, G. Scalmani and V. Barone, J. Comput. Chem., 2003, 24, 669-681.
- 52 H. Weingärtner, J. Mol. Liq., 2014, 192, 185-190.
- 53 Y. Shao, Z. Gan, E. Epifanovsky, A. T. B. Gilbert, M. Wormit, J. Kussmann, A. W. Lange, A. Behn, J. Deng, X. Feng, D. Ghosh, M. Goldey, P. R. Horn, L. D. Jacobson, I. Kaliman, R. Z. Khaliullin, T. Kuś, A. Landau, J. Liu, E. I. Proynov, Y. M. Rhee, R. M. Richard, M. A. Rohrdanz, R. P. Steele, E. J. Sundstrom, H. L. Woodcock, P. M. Zimmerman, D. Zuev, B. Albrecht, E. Alguire, B. Austin, G. J. O. Beran, Y. A. Bernard, E. Berquist, K. Brandhorst, K. B. Bravaya, S. T. Brown, D. Casanova, C.-M. Chang, Y. Chen, S. H. Chien, K. D. Closser, D. L. Crittenden, M. Diedenhofen, R. A. DiStasio, H. Do,

- A. D. Dutoi, R. G. Edgar, S. Fatehi, L. Fusti-Molnar, Ghysels, A. Golubeva-Zadorozhnaya, J. Gomes, M. W. D. Hanson-Heine, P. H. P. Harbach, A. W. Hauser, E. G. Hohenstein, Z. C. Holden, T.-C. Jagau, H. Ji, B. Kaduk, K. Khistyaev, J. Kim, J. Kim, R. A. King, P. Klunzinger, D. Kosenkov, T. Kowalczyk, C. M. Krauter, K. U. Lao, A. D. Laurent, K. V. Lawler, S. V. Levchenko, C. Y. Lin, F. Liu, E. Livshits, R. C. Lochan, A. Luenser, P. Manohar, S. F. Manzer, S.-P. Mao, N. Mardirossian, A. V. Marenich, S. A. Maurer, N. J. Mayhall, E. Neuscamman, C. M. Oana, R. Olivares-Amaya, D. P. O'Neill, J. A. Parkhill, T. M. Perrine, R. Peverati, A. Prociuk, D. R. Rehn, E. Rosta, N. J. Russ, S. M. Sharada, S. Sharma, D. W. Small, A. Sodt, T. Stein, D. Stück, Y.-C. Su, A. J. W. Thom, T. Tsuchimochi, V. Vanovschi, L. Vogt, O. Vydrov, T. Wang, M. A. Watson, J. Wenzel, A. White, C. F. Williams, J. Yang, S. Yeganeh, S. R. Yost, Z.-Q. You, I. Y. Zhang, X. Zhang, Y. Zhao, B. R. Brooks, G. K. L. Chan, D. M. Chipman, C. J. Cramer, W. A. Goddard, M. S. Gordon, W. J. Hehre, A. Klamt, Schaefer, M. W. Schmidt, C. D. Sherrill, D. G. Truhlar, A. Warshel, X. Xu, A. Aspuru-Guzik, R. Baer, A. T. Bell, N. A. Besley, J.-D. Chai, A. Dreuw, B. D. Dunietz, T. R. Furlani, S. R. Gwaltney, C.-P. Hsu, Y. Jung, J. Kong, D. S. Lambrecht, W. Liang, C. Ochsenfeld, V. A. Rassolov, L. V. Slipchenko, J. E. Subotnik, T. Van Voorhis, J. M. Herbert, A. I. Krylov, P. M. W. Gill and M. Head-Gordon, Mol. Phys., 2015, 113, 184-215.
- 54 A. D. Becke, Phys. Rev. A: At., Mol., Opt. Phys., 1988, 38, 3098-3100.
- 55 F. Weigend and R. Ahlrichs, Phys. Chem. Chem. Phys., 2005, 7, 3297-3305.
- 56 P. Eiden, S. Bulut, T. Köchner, C. Friedrich, T. Schubert and I. Krossing, J. Phys. Chem. B, 2011, 115, 300-309.
- 57 F. Neese, Wiley Interdiscip. Rev.: Comput. Mol. Sci., 2012, 2, 73-78.
- 58 F. Neese, Wiley Interdiscip. Rev.: Comput. Mol. Sci., 2018, 8, e1327.
- 59 C. Lee, W. Yang and R. G. Parr, Phys. Rev. B: Condens. Matter Mater. Phys., 1988, 37, 785-789.
- 60 S. H. Vosko, L. Wilk and M. Nusair, Can. J. Phys., 1980, 58, 1200-1211.
- 61 W. Humphrey, A. Dalke and K. Schulten, J. Mol. Graphics Modell., 1996, 14, 33-38.
- 62 A. Klamt and G. Schüürmann, J. Chem. Soc., Perkin Trans., 1993, 799-805.